Cost and CO_2 emission optimization of precast-prestressed concrete U-beam road bridges by a hybrid glowworm swarm algorithm

Víctor Yepes [1]

José V. Martí [2]

Tatiana García-Segura [3]

ABSTRACT

This paper describes a methodology to optimize cost and CO_2 emissions when designing precast-prestressed concrete road bridges with a double U-shape cross-section. To this end, a hybrid glowworm swarm optimization algorithm (SAGSO) is used to combine the synergy effect of the local search with simulated annealing (SA) and the global search with glowworm swarm optimization (GSO). The solution is defined by 40 variables, including the geometry, materials and reinforcement of the beam and the slab. Regarding the material, high strength concrete is used as well as self-compacting concrete in beams. Results provide engineers with useful guidelines to design PC precast bridges. The analysis also revealed that reducing costs by 1 Euro can save up to 1.75 kg in CO_2 emissions. The parametric study indicates that optimal solutions in terms of monetary costs have quite a satisfactory environmental outcome and differ only slightly from the best possible environmental solution obtained.

Keywords

Optimization; Glowworm swarm algorithm; Computer aided design; Structural design; Sustainable design; Precast concrete; Bridges

---

[1] Associate Professor, Institute of Concrete Science and Technology (ICITECH), *Universitat Politècnica de València*, 46022 Valencia, Spain. **Corresponding author**. Phone +34963879563; Fax: +34963877569; E-mail: vyepesp@upv.es

[2] Associate Professor, Institute of Concrete Science and Technology (ICITECH), *Universitat Politècnica de València*, 46022 Valencia, Spain. E-mail: jvmartia@upv.es

[3] Graduate Research Assistant, Institute of Concrete Science and Technology (ICITECH), *Universitat Politècnica de València*, 46022 Valencia, Spain. E-mail: tagarse@cam.upv.es

1. Introduction

Nowadays, global warming and the gradual deterioration of our planet are both cause for concern. Within the global development context, the environmental impact of construction activities is significant. While the embodied greenhouse gas (GHG) emissions were limited by the Kyoto Protocol, the construction industry continues to generate 40-50% of all global GHG emissions [1]. According to the Environmental Protection Agency (EPA), buildings are responsible for 38% of entire carbon dioxide (CO_2) emissions of the United States [2]. Furthermore, the cement industry produces 5% of world's GHG emissions [3]. Consequently, it is not enough to build cheaply and efficiently; construction should save non-renewable natural resources and respect the environment. This has promoted research related to sustainability in the field of construction.

For concrete structures, savings in CO_2 emissions can be achieved not only by recycling [4, 5] and by the use of novel materials, such as low-carbon cements and clinker substitutes [6,7], but also by decreasing the unit CO_2 emissions of each structural material in the design stage and construction processes [8]. Hasanbeigi et al. [9] collected information from publically available sources related to the production of one unit of concrete. Such inventory data are of course depending on the local conditions at the production site such as climate, energy resources, transportation distances and the general conditions of the equipment and plant facilities. Construction materials contribute about 75% of the total CO_2 emission of a construction process [10]. Turner and Collins [11] present a study including energy expending activities associated with mining and transport of raw materials, manufacturing and concrete construction for both geopolymer and Ordinary Portland Cement. García-Segura et al. [7] evaluated CO_2 emissions and CO_2 capture for a reinforced concrete structure during its service life and after demolition and reuse as gravel filling material. However, when attempting to calculate the CO_2 emission consideration about construction methods or processes are usually not incorporated in those calculations. The transport of batched concrete as well as on-site placement activities such as pumping, vibrating and finishing concrete consumes diesel fuel. Nevertheless, these construction activities were all found to contribute very small amounts of CO_2 to total concrete emissions [10].

Hence, the importance of incorporating design criteria to minimize emissions in the construction of concrete structures. To this end, databases measuring the materials-environmental impact have been

elaborated [12-14]. These databases have been used by Paya-Zaforteza et al. [15] and Yepes et al. [16] to conduct studies comparing optimization designs based on the CO_2-efficiency and the cost-design for reinforced concrete (RC) building frames and walls. Camp and Assadollahi [17] and Camp and Huq [18] have optimized the CO_2 and the structural cost of RC footings and frames, respectively. Park et al. [19] suggested an optimization technique for steel reinforced concrete columns in high-rise buildings that simultaneously considers the structural cost and CO_2 emissions at the structural design phase. Yeo and Potra [20] carried out a similar study for RC moment frames, while Medeiros and Kripka [21] proposed the minimization of monetary and environmental costs of rectangular RC column sections. The work of Fernandez-Ceniceros et al. [22] presents a decision criterion based on the embodied CO_2 and the overall cost of one-way floor slabs. This paper addresses the sustainability challenge by incorporating the CO_2 emission objective in the search for the optimum design of precast-prestressed concrete U-beam road bridges.

In this context, precast construction presents social and environmental benefits [23] and has proved worthwhile when high production volumes are possible leading to the corresponding savings in costs and construction time. Horvarth and Herndrickson [24] found that for the initial construction of equivalent bridge girders for a particular location, a steel-reinforced concrete bridge generally has lower environmental effects than a steel bridge despite the fact that the uncertainty in bridge design life and related data uncertainties make comparisons based on annualized environmental effects difficult. Most Spanish road bridges are constructed with precast prestressed concrete (PC) beams. Precast PC beam decks are more common in other European countries and the United States. This typology is generally used when longer distances are involved. This is the case of the world's longest bridge (The Danyang-Kunshan Grand Bridge, 2011), which is a 164.8-kilometer long viaduct with 80 m spans. The longest bridge in the United States is the Lake Pontchartrain Causeway (1956) which is 38.4 km and has 45.7 m spans making it the seventh in the world ranking. For this reason, structural optimization of this type of large and repetitive structures is an area of much research interest given the large amount of materials required in the manufacturing process.

PC beam optimization is a classical problem considered many years ago [25]; nevertheless, as Hernandez et al. [26] have advised, most approaches for PC bridges found in the literature are not suitable for application in real life engineering. While there is little research on optimization of PC structures [27-31], the literature does include a number of studies on optimizing real-life reinforced concrete (RC)

structures [32-36]. Ohkubo et al. [27] studied prestressed concrete box girder bridges and proposed a multicriteria fuzzy optimization of the total construction cost and aesthetic feeling. Sirca and Adeli [28] and Ahsan et al. [29] focused on the cost optimum design of concrete I-girder bridges. Both used precast and prestressed concrete for the beams, the latter also used post-tensioned tendons. An earlier paper written by the authors [30] optimized the cost of prestressed concrete precast U-beam road bridges, but with certain differences which are mentioned in further detail below. Semelawy et al. [31] carried out an optimization of a pre-stressed concrete slab using the cost and the distance from the constraint boundary as objective functions. However, little attention has been paid to the CO_2 emissions optimization of PC structures. In this context, the best results found for many real-life problems are obtained by hybrid algorithms [37]. The main motivation behind the hybridization of different algorithms is to exploit the complementary character of different optimization strategies. Blum et al. [38] provided a survey on the hybridization of metaheuristics with other techniques for combinatorial optimization problems.

In this study, an optimal design method is presented which minimizes the CO_2 emissions and cost for structural design of PC precast road bridges. The use of these U-beams in an overpass is considered more aesthetically pleasing than a comparable bridge of I-beams as fewer beam lines are needed, improving the appearance as viewed from below. Moreover, this type of bridge beam is cost-competitive with other concrete beams due to the exceptional resistance capacity and load-bearing capacity element weight ratio. These bridges are typically formed by two isostatic beams (Fig. 1), with a double U-shape cross-section that integrates a 12 m width upper reinforced concrete slab for road traffic (Fig. 2). Beams use self-compacting concrete (SCC), as well as high strength concrete which can also be used in the slab as an innovative aspect. This type of bridge has the advantages of a prefabricated structure, such as industrial construction, reusable formwork, reduced labor times and low interference with traffic. The methodology followed in this study consisted in developing a computer evaluation module from the cross-section dimensions, materials and steel reinforcement. This module computed the CO_2 emissions of a solution and checked all the relevant limit states. The proposed optimal design method employs a hybrid glowworm swarm optimization algorithm as an optimization tool. This algorithm combines the GSO algorithm with the SA local search. The objective function of CO_2 emission is evaluated along with the economic cost during the bridge materials production and manufacture, transport and construction.

2. Problem definition

2.1. Optimization problem definition

The structural design problem established for this research aims to minimize the objective function F of Eq. (1), subject to the constraints represented by Eq. (2).

$$F(x_1, x_2, ..., x_n) \quad (1)$$

$$g_j(x_1, x_2, ... x_n) \leq 0 \quad (2)$$

$$x_i \in \left(d_{i1}, d_{i2}, ..., d_{iq_i} \right) \quad (3)$$

Note that $x_1, x_2, . . ., x_n$ are the variables to be optimized (design variables). Each design variable may assume the discrete values listed in Eq. (3). The objective function F defined in Eq. (1) is either the CO_2 emission or the cost. The constraints g_j in Eq. (2) are all the service limit states (SLSs) and ultimate limit states (ULSs) with which the structure must comply, as well as the geometric and constructability requirements of the problem.

This study analyzes sustainability based on a function of CO_2 emissions during the construction process. To this end, the values for materials were taken from the database BEDEC [14]. Applying a CO_2 emission to each unit in which the construction is split leads to a comparative analysis of the alternatives from an environmental point of view. It is assumed that the steel is mainly made by the electric arc furnace, approximately 40% from recycled scrap steel. The CO_2 emissions are defined in Eq. (4), where e_i are the unit emissions (Tables 1 and 2) depending on the design variables, and m_i are the measurements for the total number of construction units r. Note that concrete unit emissions were determined from each mix design. The emissions from the production of cement, aggregate, and water were obtained from the database BEDEC [14]. The plasticizer [39] and superplasticizer [40] were taken from the European Federation of Concrete Admixtures Associations. Regarding the silica fume, this study considers that a waste product does not produce emissions [41]. The beam concrete emissions include the use of admixtures in order to accelerate the curing process. The slab concrete emissions include the transport and placement emissions. However, the beam transport and placement were considered separately (see Table 2), since this depends on the beam length [14].

$$CO_2 = \sum_{i=1,r} e_i \times m_i \quad (4)$$

The cost is defined in Eq. (5), where p_i are unit prices and m_i are measurements. The cost function includes the materials (concrete, active prestressing steel, passive reinforcement steel) and all the elements to evaluate the entire cost of the bridge construction. Unit prices were obtained from a survey of Spanish contractors and subcontractors of precast structures and adapted to current prices. The values are given in Tables 1, 3 and 4 [42].

$$C = \sum_{i=1,r} p_i \times m_i \qquad (5)$$

2.2. Design variables and parameters

The structural geometry and materials are defined by 40 variables. Eight variables define the geometry (see Fig. 3): the depth of the beam (h_1), the width of the soffit of the beam (b_1) and the thickness of the bottom flange (e_1), the width and thickness of the top flanges of the beam (b_3 and e_3), the thickness of the webs (e_2), the thickness of the slab (e_4) and the spacing between beams (s_v). Two variables define the concrete type for the slab and the beam. Prestressing, which is formed by 0.6 in. strands, is defined by four variables: the number of strands in the top flanges and the number of strands in the first, second and third layers of the bottom flange. Finally, 26 variables define the bar diameters, the spacing and the bar lengths of the reinforcement following a standard set-up for the beam and the top slab. The parameters are all fixed quantities that do not change during the optimization. Table 5 lists the 21 main parameters analyzed. The former paper written by the authors [30] does not include the separation between beams (S_v) as well as high-strength concrete for beams and slabs.

2.3. Structural evaluation module

The structural evaluation module calculates the stress envelopes and checks all the limit states and the geometric constraints represented by Eq. (2). Structural constraints as well as the combination of actions follow standard provisions for the Spanish design of this type of structure [43,44] and include checks of the serviceability and ULSs of flexure and shear for the stress envelopes due to the loads. IAP-98 [43] was considered to determine the variable actions applied to the deck. However, it should be noted that recently these actions have been changed to adapt to the Eurocode content. The design live load consists of three axis of 200 kN each (1.5 m distance between axes), superimposed with a uniform load of 4.0 kN/m^2. The dead load is a wearing surface of 0.09 m as well as a uniformly distributed load of 2x0.5 kN/m for concrete bridge barrier rails installed along the edge of the deck. The combinations of actions

include all construction stages. Laminated neoprene bearing pads are used to support the precast concrete bridge beams. A single support point is used at each end of the beam. The pads are designed to carry vertical loads and to accommodate horizontal movements of the bridge girders. They are also designed to deflect horizontally under shearing-type forces. The slenderness of the beam (span length over beam depth) is limited to a minimum of $L/17$ due to aesthetic, ground and specific road transportation considerations, where L is the span length. A 20-bar element structural model was first used for a linear elastic analysis of the beam before being connected to the slab; then, stress resultants and reactions are calculated by a stiffness matrix program using a 2-D mesh with 20 bar elements and 21 sections for each beam, which are connected with three bar elements for each of the 21 sections. The entire bar model has 103 bar elements and 84 nodes, for which a linear elastic analysis including gross section properties is used. The construction sequences and the long-term interaction between the precast beam and the cast-in-place concrete were considered to design the elements and analyze the structural response of the bridge in each phase. The details of the structural model can be found in the work by Martí et al. [30].

The ULSs and SLSs are checked in accordance with the Spanish Concrete Code [44] when the deflections and the envelopes of stress resultants are known. The reinforcement verification procedure does not follow the usual design rule. The indicated rule is an iterative method obtaining reinforcement bars from flexural-shear ULSs and checking SLSs. Heuristic algorithms can find new economical reinforcement solutions, for instance, suppressing shear reinforcement by increasing flexural reinforcement. ULS verification implies that the ultimate values are greater than the factored acting. Besides, both flexural and shear minimum amounts of reinforcement, as well as the geometric minimum, are also tested. Regarding flexure in beams, the acting bending resultant, M_d, is checked to assure that it is within the ultimate iteration diagram N_u–M_u. The SLS for cracking includes conformity with the crack width limitation for durability conditions. In addition, fatigue of concrete and steel was considered. Temporary deflections were limited to 1/250 of the free span length for the frequent combination. Further, time-dependent deflections were limited to 1/1000 of the free span length for the quasi-permanent combination. Finally, the durability limit state requires compliance of the service working life.

3. Hybrid glowworm swarm optimization algorithm

GSO was proposed by Krishnanand and Ghose [45] to find solutions for the optimization of multiple optima continuous functions. GSO is a swarm intelligence algorithm based on the collective behavior of

glowworms interacting locally. Each glowworm is attracted and moves toward another glowworm that is in its neighborhood and glows brighter. The quantity of luminescence is called luciferin. The luciferin level depends on the fitness of its location, which is evaluated using the objective function. The neighborhood is encoded by a dynamic radial rate, which requires calibration. Glowworms decide by a probabilistic function the glowworm toward which it will move. However, GSO-based algorithms present three main drawbacks: the glowworms may get stuck in local optima; they fall easily into an unfeasible solution, and they have slow convergence rates. To overcome these drawbacks, a hybridized method combining simulated annealing and glowworm swarm optimization (SAGSO) algorithms is used. SAGSO uses SA optimization after every glowworm movement to ensure feasibility of the solution and to accelerate convergence to the optimum. This algorithm was simultaneously used for the first time by our research group in this paper as well as on optimizing reinforced concrete I-beams [41], which outperformed conventional GSO and SA independently in terms of both the quality and the computing time.

SA was originally proposed by Kirkpatrick et al. [46] to design electronic circuits. This algorithm is based on the analogy of crystal formation from masses melted at high temperatures and cooled slowly to allow atoms to align themselves reaching a minimum energy state. The probability of accepting new solutions is governed by the expression $exp(-\Delta E/T)$, where ΔE is the increment in energy of the new configuration and T is the temperature. The increment in energy is evaluated according to the objective function. The initial temperature decreases geometrically $(T = kT)$ by means of a coefficient of cooling k once a Markov chain M_c ends. The initial temperature T_0 is usually adjusted following methods like that proposed by Medina [47], which consists of choosing an initial value and checking the percentage of higher energy solutions accepted. If this percentage is greater than 40%, the initial temperature is halved; when it is less than 20%, the initial temperature is doubled. Fig. 4 shows a flowchart of the simulated process. The algorithm ends when the number of iterations t reaches the maximum t_{max}. The procedure can be summarized as follows:

1. Initially, a swarm of n feasible glowworms is randomly generated. They are distributed in the search space. The initial luciferin value l_0 and the initial radial sensor range r_s is assigned to each glowworm. After calculating each objective function, the worst F_{max} is chosen.

2. The luciferin value update depends on the previous luciferin l_i and the objective function value F(x_i), as shown in Eq. (6). The luciferin value decay constant ρ ($0 < \rho < 1$) simulates the

decrease in luciferin level over time, and the luciferin enhancement constant γ ($0 < \gamma < 1$) is the proportion of the improvement in the objective that the glowworm adds to its luciferin.

$$l_i(t + 1) = (1 - \rho)l_i(t) + \gamma(F_{max} - F(x_i(t + 1)))$$ (6)

3. The glowworm decides, by a probabilistic function, which glowworm it will target for movement. This probability is given by Eq. (7). $N_i(t)$ is the set of neighbors of glowworm i at the iteration t. The neighbors must have higher values of luciferin; they must be located within the radial sensor range $r^i_d(t)$, and they must be feasible solutions. Distance d_{ij} represents the Euclidean distance between glowworms i and j.

$$p_{ij}(t) = \frac{l_j(t)\text{-}l_i(t)}{\sum_{k \in N_i(t)} l_k(t)\text{-}l_i(t)}$$ (7)

4. During the movement phase, the glowworm i moves toward the chosen glowworm j. The following Eq. (8) defines the discrete position of the new value of the variable, where s (>0) is the step size.

$$x_i(t + 1) = int\left(x_i(t) + s\left(\frac{x_j(t)\text{-}x_i(t)}{d_{ij}}\right)\right)$$ (8)

where $j \in N_i(t), N_i(t) = \{j : d_{ij} < r^i_d(t); l_i(t) < l_j(t)\}$

5. Once the movement is finished, the radial sensor range is updated in Eq. (9) according to the constant parameter β and a parameter to control the number of neighbors n_t. The new solution is checked and evaluated. Even if the new solution is unfeasible, it is accepted. In this case, the objective function is penalized.

$$r^i_d(t + 1) = \min\left\{r_S, \max\{r^i_d(t) + \beta(n_t\text{-}|N_i(t)|\}\right\}$$ (9)

6. A total of n_M Markov chains are run. A percentage of the variables (n_p) are modified by a small random movement.

7. The solution is evaluated. Only feasible solutions whose probabilities are greater than a random number between 0 and 1 are accepted.

$$random < e^{\frac{J(x_i(t)\text{-}J(x_i(t+1)}{T}}$$ (10)

8. When the Markov chain ends, the temperature decreases following Eq. (11). Therefore, the probability of accepting worse solutions also decreases.

$$T = kT$$ (11)

The hybrid glowworm swarm optimization algorithm requires the definition of certain parameters (t_{max}, n, n_t, l_o, r_s, ρ, γ, β, s, n_M, k, Mc, n_p). To find the proper heuristic which increases the solution quality and improves the global searching capability, the algorithm was run several times and the parameters are randomly generated. Further, computer runs were performed nine times for each combination according to the methodology proposed by Payá-Zarforteza et al. [48] based on the extreme value theory. A span length of 35 m was considered. Fig. 5 and Fig. 6 show, respectively, the best solutions for cost and CO_2 emissions and the computing time for each combination. Table 6 gives the results of a six case-study series whose results are optimal when both CO_2 emissions and computing time are considered. S1 is the heuristic that provides a lower minimum emission (170,002.39 kg CO_2). Besides, the average emission and computing time are reasonable. The difference checked between the minimum CO_2 emissions obtained with the nine SAGSO runs and the extreme value estimated using the three-parameter Weibull distribution that fits 50 SAGSO results is less than 0.7%. So, this set of parameter is chosen. Similarly, Table 7 gives the results for the parameters calibration using cost as objective function. Note that our previous test for a span length of 35 m showed that the best results for the GSO and SA algorithms were 218,264.59 kg CO_2 and 182,652.04 kg CO_2, respectively.

4. Results from numerical experiments and parametrical study

In this Section, we examine the results from numerical experiments involving SAGSO optimization applied to a PC precast road bridge. The algorithm was coded in Intel® Visual Fortran Compiler Integration for Microsoft Visual Studio 2010. A personal computer with an INTEL® Core[TM] i7-3820 CPU processor and 3.6 GHz needed about 500 min to run the proposed SAGSO algorithm. Computer runs were performed nine times so as to obtain minimum, average and standard deviation.

A parametric study for varying span lengths is presented. It is assumed that the cost and CO_2 emissions are specified (Tables 1-4). The primary economic (cost and CO_2 emissions) and geometric characteristics are examined. The results lead to practical rules for the preliminary design of optimized PC precast road bridges, with a double U-shaped cross-section and isostatic spans. The corresponding functions are valid approximations within the range of the studied parameters, and therefore, careful consideration is required when extrapolated.

Fig. 7 and Fig. 8 show, respectively, the average value variation in the minimum cost and CO_2 emissions (for cost and CO_2 objective) for five span lengths (s), ranging from 20 to 40 m in steps of 5 m.

The minimum emissions and costs rise with increasing bridge span lengths. The average difference between the mean value of the results and the minimum value found after nine runs is only 2.9% for emissions and 1.8% for costs. These differences are sufficiently low for practical applications. A parabolic relation may be used to describe the general cost trend for both cost-optimized solutions ($C=48.088s^2+613.99s+31139$ with a regression coefficient $R^2=0.9999$) and emission-optimized solutions ($C=55.99s^2+163.96s+39134$ with $R^2=0.9998$). Similarly, the general emission trend is represented by a parabolic function for both cost-optimized solutions ($kgCO_2=63.878s^2+2429.3s+13052$ with $R^2=1$) and emission-optimized solutions ($kgCO_2=63.418s^2+2392.3s+13328$ with $R^2=0.9999$).

Fig. 9 depicts the relationship between the best values for the emissions and cost when the objective function is either the amount of CO_2 or the monetary cost. It is possible to observe a linear fit between emissions and cost ($kgCO_2=1.7533C-25153$ with $R^2=0.9988$ for emission-optimized solutions) which indicates that, as a rule of thumb, reducing costs by 1 Euro results in savings of 1.75 kg in CO_2 emissions. This relationship assumes standard technology to assess the emissions of each construction unit. For example, if a different mixture composition is used, there will be an increase or decrease in concrete composition materials, and such changes should be taken into consideration when calculating the amount of CO_2. Nevertheless, this relationship suggests that the optimization of monetary costs is closely related to a reduction in environmental costs. This has already been reported by Paya-Zaforteza et al. [15] for CO_2-optimization of RC building frames as well as by Yepes et al. [16] for RC retaining walls. This is a significant finding since clearly reducing CO_2 emissions is economically affordable with regard to reducing global warming. Moreover, prices are more sensitive to market cycles, while emissions depend on stricter manufacturing processes. Therefore, it appears that designs based on emissions are more stable and more rational. However, the physical dimensions and details of the design for cost and emissions optimization can vary significantly because unit prices and emissions are not in any proportional relationship to one another.

Fig. 10 shows a good linear variation between the beam depth and the span length of the bridge. The average depth of the beam is 1/18.08 in relation with the span, when the objective is to reduce the emissions. This value is similar to 1/17.57 which corresponds to the cost optimization. The reason for this is that the ratio L/h_1 is always lower than 17 (see Table 5). As shown in Fig. 11, values for slab thickness decrease with the span length when the objective is to reduce the CO_2 emissions. However, this relationship only occurs when the value for the span length is less than 35 m in the case of reducing cost.

In addition, Fig. 11 shows no clear difference in values for slab thickness between the cost-optimized and the emission-optimized design.

Regarding the average number of strands in relation to the span, Fig. 12 illustrates a linear correlation for the span length of the bridge. Results are quite similar for both objective functions. Fig. 13 shows the relation between the concrete strength and the span length. There is a clear trend toward increasing concrete strength as the span lengthens, so as to lighten the load. If emission is optimized, concrete strength values decreased compared to cost objective. Despite the fact that high-strength concrete is usually used for precast-prestressed concrete, note that concrete strength for short spans tends to be the minimum proposed (25 MPa for slabs and 35 MPa for beams). However, for the maximum span length studied, even with the concrete strength increase, it is far from the highest (100 MPa). Regarding the ratio of the mean spacing between beams, there is no a clear tendency with the span length, but in every case the spacing is less than half of bridge width (Fig. 14); what is more, there is no clear difference in values for the spacing between the cost-optimized and the emission-optimized design. Table 8 summarizes the amount of passive reinforcement and concrete in beams and slabs. Passive reinforcement increases with the span length, being greater in emission-optimized beams and cost-optimized slabs. The average amounts in beams and slabs are 5205 kg and 8846 kg, respectively, for the minimum emission and 4833 and 10898 for the minimum cost. This represents an average of 37.04 kg/m^2 of deck for the emission case and 42.35 kg/m^2 of deck for the cost. Regarding the concrete required in beam, an increase is observed according to the span, being greater for emission optimization. However, slab concrete, as noted in Fig. 11, decreases with the span length. In this case, lower values were obtained for the best cost option.

Finally, SAGSO was applied to a PC precast bridge with a 35 m span with various scenarios of the material cost. Figure 15 indicates that the cost impact is greater when the unit price increase occurs in the steel. Thus, a maximum 20% rise in the steel unit price leads to 10.27% increase in the cost, while 20% rise in the concrete unit price increases the cost up to 3.41%. Figure 16 shows a decrease in the steel quantity in accordance with a higher steel cost whereas an increase in the concrete cost results in a slight increase in the steel quantity. In addition, Figure 17 shows a rise in the volume of concrete when the steel price rises; surprisingly, in this case, the variation in the volume of concrete is almost insensitive to its rising price.

5. Conclusions

In this paper, a hybrid method combining simulated annealing with glowworm swarm optimization (SAGSO) algorithms is presented and employed to optimize PC precast road bridges formed by two isostatic beams with a double U-shaped cross-section. Two objective functions are considered: the CO_2 emissions and cost of the PC bridge at the different stages of material production, transportation and construction. The extensive computational experiments with a set of five span lengths for the bridge indicate that SAGSO is an efficient algorithm for the advanced automatic design of real PC precast bridges used in road construction that reduced the CO_2 emissions and the cost. The analysis reveals that CO_2 emissions and cost are closely related and, as a rule of thumb, a euro reduction in cost results in savings of 1.75 kg in CO_2 emissions. Thus, the solutions which are acceptable for emissions are also viable in terms of cost and vice versa. The parametric study shows a good correlation for both the depth of the beam, the thickness of the slab, the number of strands and the characteristic compressive strength of concrete, which can be useful for the day-to-day design of PC precast bridges. Greater and lesser amounts of passive reinforcement are observed in the beams and the slab, respectively, for CO_2-optimization. Regarding concrete, larger volumes are used when optimizing the emission. It must be noted that the repetition of the PC structures increases the economic savings. A cost sensitivity analysis applied to a PC precast bridge with a 35 m span indicates that a maximum 20% rise in steel costs leads to a 10.27% increase in the cost, while a 20% rise in concrete costs only increases the cost up to 3.41%; surprisingly, the variation in the volume of concrete is almost insensitive to its rising price. To conclude, this hybrid method, described herein, is quite flexible and can easily be modified and extended so that structural engineers may reduce CO_2 emissions in their structural designs.

Acknowledgments

References

[1] CIWMB, Designing with vision: a technical manual for material choices in sustainable construction. California Integrated Waste Management Board, Sacramento, 2000.

[2] J.S. Damtoft, J. Lukasik, D. Herfort, D. Sorrentino, E.M. Gartner, Sustainable development and climate change initiatives, Cem. Concr. Res. 38 (2) (2008)115-127.

[3] E. Worrell, L. Price, N. Martin, C. Hendriks, L.O. Meida, Carbon dioxide emissions from the global cement industry, Annu. Rev. Energy Env. 26 (2001) 303-329.

[4] F. Collins, Inclusion of carbonation during the life cycle of built and recycled concrete: influence on their carbon footprint, Int. J. Life Cycle Assess. 15 (6) (2010) 549-556.

[5] M. Yellishetty, G.M. Mudd, P.G. Ranjith, A. Tharumarajah, Environmental life-cycle comparisons of steel production and recycling: sustainability issues, problems and prospects, Environ. Sci. Policy 14 (6) (2011) 650-663.

[6] E.M. Gartner, Industrially interesting approaches to "low-CO_2" cements, Cem. Concr. Res. 34 (9) (2004) 1489-1498.

[7] T. García-Segura, V. Yepes, J. Alcalá, Life cycle greenhouse gas emissions of blended cement concrete including carbonation and durability, Int. J. Life Cycle Assess. 19 (1) (2014) 3-12.

[8] J.K.W. Wong, H. Li, H. Wang, T. Huang, E. Luo, V. Li, Toward low-carbon construction processes: the visualisation of predicted emission via virtual prototyping technology, Automation in Construction 33 (2013) 72-78.

[9] A. Hasanbeigi, L. Price, E. Lin, Emerging energy-efficiency and CO_2 emission-reduction technologies for cement and concrete production: A technical review, Renew. Sust. Energ. Rev. 16 (8) (2012) 6220-6238.

[10] D.J.M. Flower, J.G. Sanjayan, Greenhouse gas emissions due to concrete manufacture, Int. J. Life Cycle Assess. 12(5) (2007) 282-288.

[11] L.K. Turner, F.G. Collins, Carbon dioxide equivalent (CO2-e) emissions: A comparison between geopolymer and OPC cement concrete, Constr. Build. Mater. 43 (2013) 125-130.

[12] M. Goedkoop, R. Spriensma, The Ecoindicator 99: A damage oriented method for life cycle impact assessment. Methodology Report, PRé Consultants, Amersfoort, Netherlands, 2001.

[13] A. Alcorn, Embodied energy and CO_2 coefficients for NZ building materials, Center for Building Performance Research, Wellington, New Zealand, 2003.

[14] Catalonia Institute of Construction Technology, BEDEC PR/PCT ITEC materials database, 2009. <http://www.itec.es/nouBedec.e/presentaciobedec.aspx> (December 14, 2013)

[15] I. Payá-Zaforteza, V. Yepes, A. Hospitaler, F. Gonzalez-Vidosa, CO_2-optimization of reinforced concrete frames by simulated annealing, Eng. Struct. 31 (7) (2009) 1501-1508.

[16] V. Yepes, F. González-Vidosa, J. Alcalá, P. Villalba, CO_2-optimization design of reinforced concrete retaining walls based on a VNS-threshold acceptance strategy, J. Comput. Civ. Eng. 26 (3) (2012) 378-386.

[17] C.V. Camp, A. Assadollahi, CO_2 and cost optimization of reinforced concrete footings using a hybrid big bang-big crunch algorithm, Struct. Multidisc. Optim. 48 (2) (2013) 411-426.

[18] C.V. Camp, F. Huq, CO_2 and cost optimization of reinforced concrete frames using a big bang-big crunch algorithm, Eng. Struct. 48 (2013) 363–372.

[19] H.S. Park, B. Kwon, Y. Shin, Y. Kim, T. Hong, S.W. Choi, Cost and CO_2 emission optimization of steel reinforced concrete columns in high-rise buildings, Energies 6 (11) (2013) 5609-5624.

[20] D. Yeo, F.A. Potra, Sustainable design of reinforced concrete structures through CO_2 emission optimization, J. Struct. Eng. B4014002 (2014) 1-7.

[21] G.F. Medeiros, M. Kripka, Optimization of reinforced concrete columns according to different environmental impact assessment parameters, Eng. Struct. 59 (2014) 185-194.

[22] J. Fernandez-Ceniceros, R. Fernandez-Martinez, E. Fraile-Garcia, F.J. Martinez-de-Pison, Decision support model for one-way floor slab design: A sustainable approach, Automation in Construction 35 (2013) 460-470.

[23] A.A. Yee, Social and environmental benefits of precast concrete technology, PCI J. 46(3) (2001) 14-20.

[24] A. Horvath, C. Hendrickson, Steel versus steel-reinforced concrete bridges: Environmental assessment, J. Infrastruct. Syst. 4 (3) (1998) 111-117.

[25] U. Kirch, Optimized prestressing by linear programming, Int. J. Numer. Methods Eng. 7 (2) (1973) 125-136.

[26] S. Hernández, A.N. Fontan, J. Díaz, D. Marcos, VTOP. An improved software for design optimization of prestressed concrete beams, Adv. Eng. Softw. 41 (3) (2010) 415-421.

[27] S. Ohkubo, P.B.R. Dissanayake, K. Taniwaki, An approach to multicriteria fuzzy optimization of a prestressed concrete bridge system considering cost and aesthetic feeling, Struct. Optim. 15 (2) (1998) 132-140.

[28] G.F. Sirca, H. Adeli, Cost optimization of prestressed concrete bridges, J. Struct. Eng. 131 (3) (2005) 380-388.

[29] R. Ahsan, S. Rana, S. Ghani, Cost optimum design of posttensioned I-girder bridge using global optimization algorithm, J. Struct. Eng. 138 (2) (2012) 273-284.

[30] J.V. Martí, F. González-Vidosa, V. Yepes, J. Alcalá, Design of prestressed concrete precast road bridges with hybrid simulated annealing, Eng. Struct. 48 (2013) 342-352.

[31] M. El Semelawy, A.O. Nassef, A.A. El Damatty, Design of prestressed concrete flat using modern heuristic optimization techniques, Expert Syst. Appl. 39(5) (2012) 5758-5766.

[32] C. Perea, J. Alcalá, V. Yepes, F. González-Vidosa, A. Hospitaler, Design of reinforced concrete bridge frames by heuristic optimization. Adv. Eng. Softw. 39 (8) (2008) 676-688.

[33] V. Yepes, J. Alcalá, C. Perea, F. González-Vidosa, A parametric study of optimum earth retaining walls by simulated annealing, Eng. Struct. 30 (3) (2008) 821-830.

[34] F.J. Martínez, F. González-Vidosa, A. Hospitaler, V. Yepes, Heuristic optimization of RC bridge piers with rectangular hollow sections, Comput. Struct. 88 (5-6) (2010) 375-386.

[35] A. Carbonell, F. González-Vidosa, V. Yepes, Design of reinforced concrete road vaults by heuristic optimization, Adv. Eng. Softw. 42 (4) (2011) 151-159.

[36] M.M. Jahjouh, M.H. Arafa, M.A. Alqedra, Artificial Bee Colony (ABC) algorithm in the design optimization of RC continuous beams, Struct. Multidisc. Optim. 47 (6) (2013) 963-979.

[37] E.G. Talbi, A taxonomy of hybrid metaheuristics, J. Heuristics 8(5) (2002) 541–564.

[38] C. Blum, J. Puchinger, G.R. Raidl, A. Roli, Hybrid metaheuristics in combinatorial optimization: A survey, Appl. Soft. Comput. 11(6) (2011) 4135-4151.

[39] EFCA. Environmental Product Declaration (EPD) for Normal Plasticising admixtures. Environmental Consultant, Sittard, 2006. <http://www.efca.info/downloads/324%20ETG%20Plasticiser%20EPD.pdf> (October 28, 2013).

[40] EFCA. Environmental Product Declaration (EPD) for Superplasticising admixtures. Environmental Consultant, Sittard, 2006. <http://www.efca.info/downloads/325%20ETG%20Superplasticiser%20EPD.pdf> (October 28, 2013).

[41] T. García-Segura, V. Yepes, J.V. Martí, J. Alcalá, Optimization of concrete I-beams using a new hybrid glowworm swarm algorithm, Lat. Am. J. Solid. Struct. 11(7) (2014) 1190-1205.

[42] J.V. Martí, Optimal design bridges boards of prestressed concrete precast beams, Doctoral thesis, Universitat Politècnica de València, Construction Engineering Dept., Valencia, Spain, 2010. [in Spanish]

[43] Ministerio de Fomento, IAP-98: Code on the actions for the design of road bridges, Ministerio de Fomento, Madrid, Spain, 1998. [in Spanish]

[44] Ministerio de Fomento, EHE-08: Code on structural concrete, Ministerio de Fomento, Madrid, Spain, 2008. [in Spanish]

[45] K.N. Krishnanand, D. Ghose, Glowworm swarm optimisation: a new method for optimising multi-modal functions, Int. J. Comp. Intell. Stud. 1 (1) (2009) 93-119.

[46] S. Kirkpatrick, C.D. Gelatt, M.P. Vecchi, Optimization by simulated annealing, Science 220 (4598) (1983) 671-680.

[47] J.R. Medina, Estimation of incident and reflected waves using simulated annealing, J. Waterway Port Coast Ocean Eng. 127 (4) (2001) 213-221.

[48] I. Payá-Zaforteza, V. Yepes, F. González-Vidosa, A. Hospitaler, On the Weibull cost estimation of building frames designed by simulated annealing, Meccanica 45(5) (2010) 693-704.
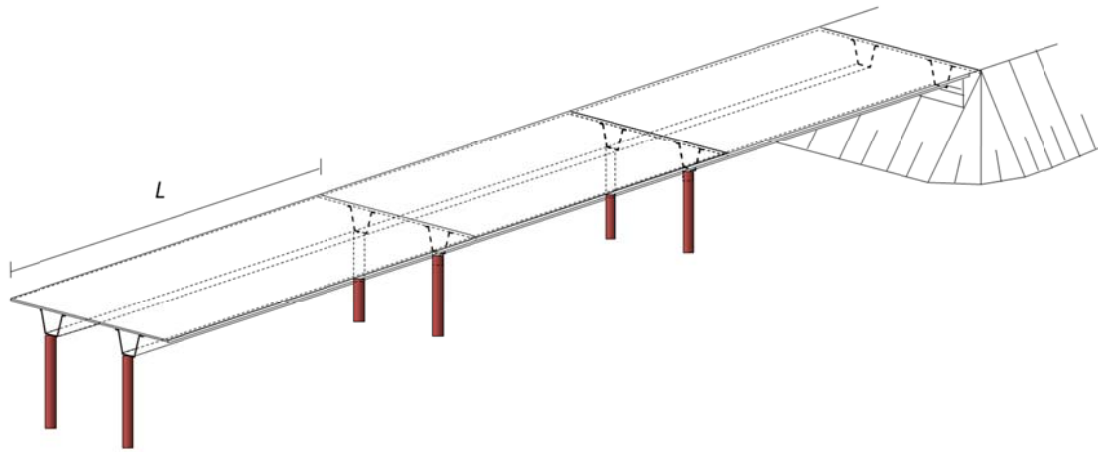
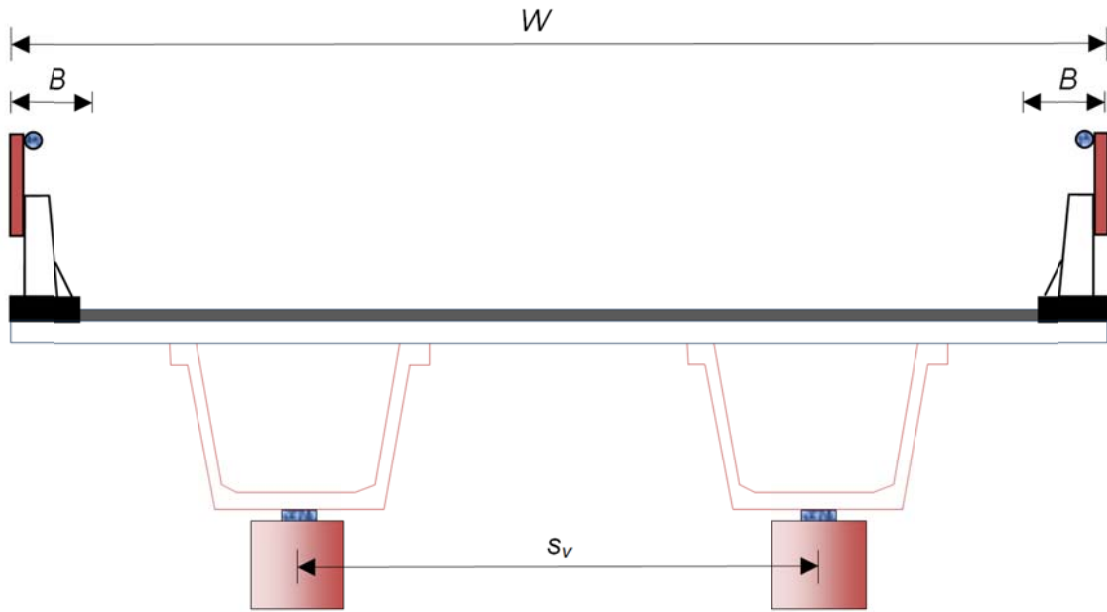**Fig. 1.** PC precast road bridge longitudinal profile

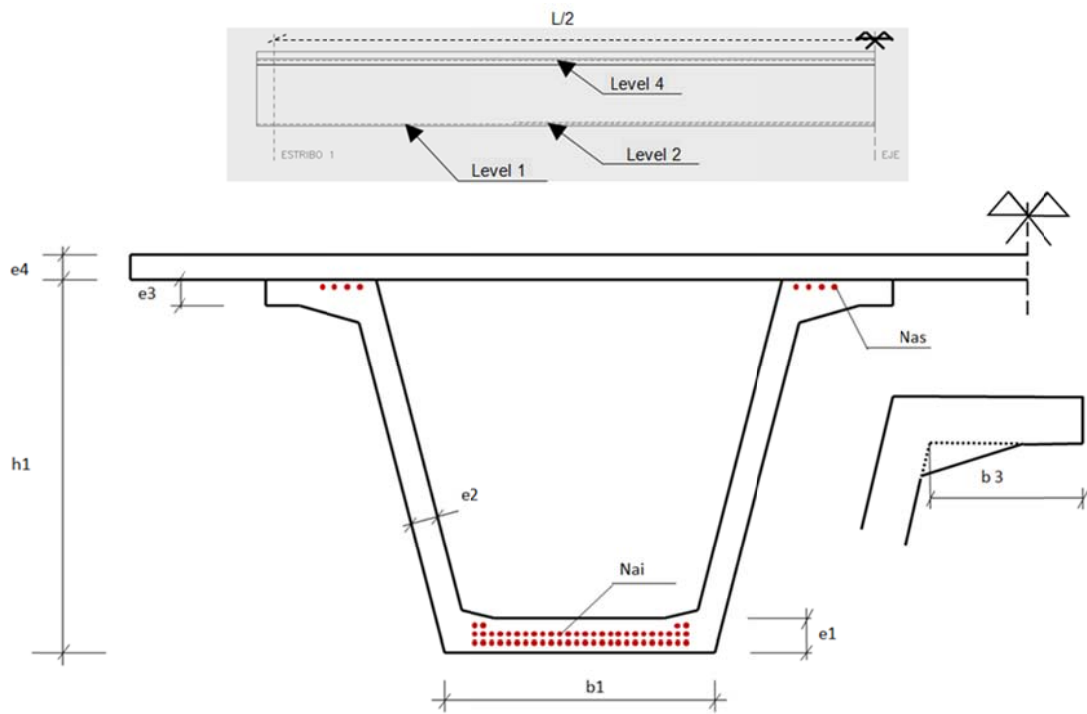**Fig. 2.** Double U-shape cross-section

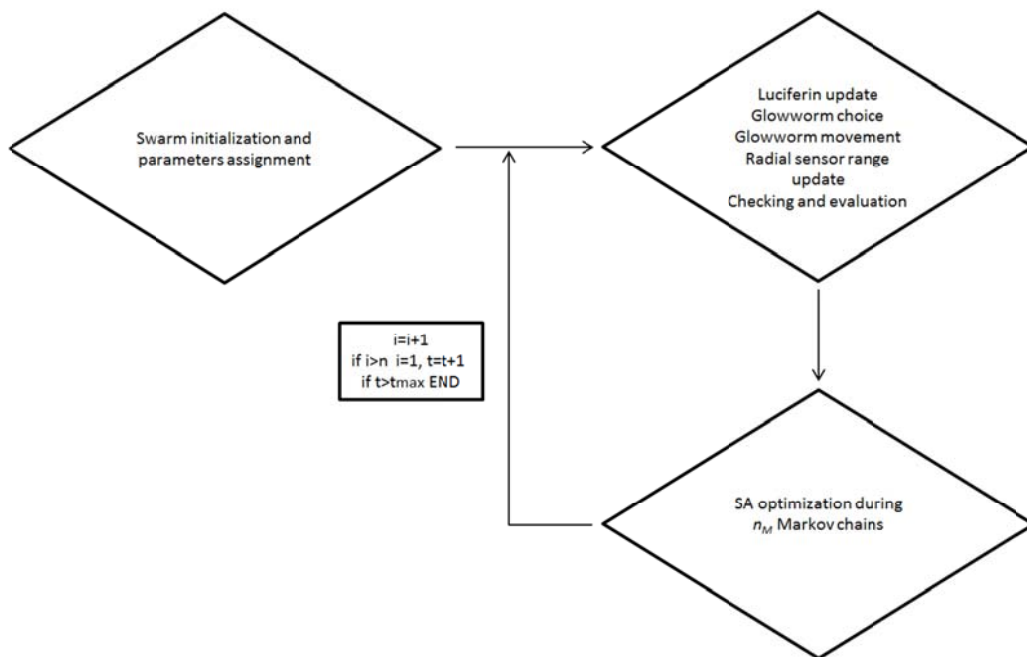**Fig. 3.** Design variables for the PC precast road bridge

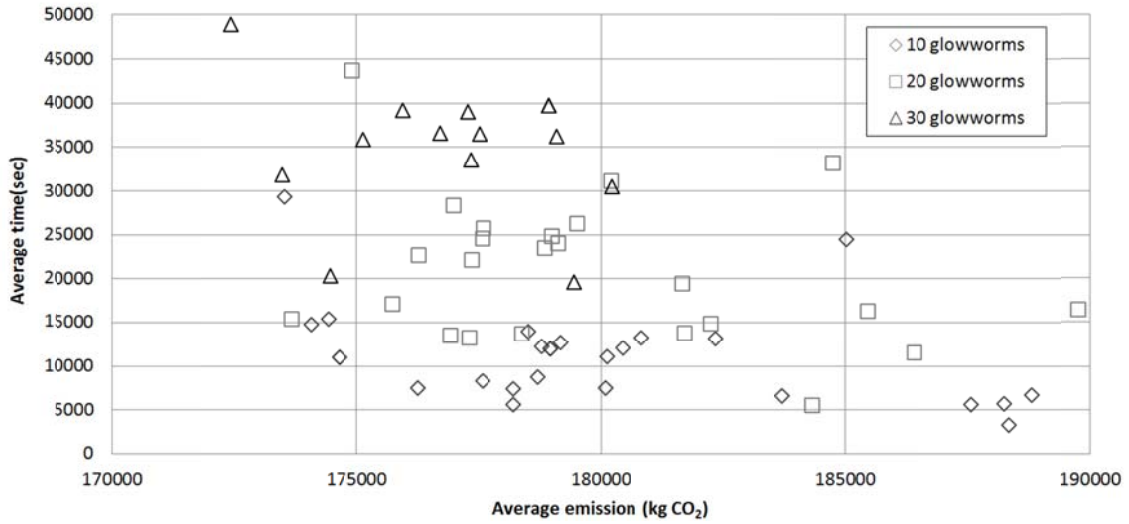**Fig. 4**. Flowchart for the proposed SAGSO optimization technique

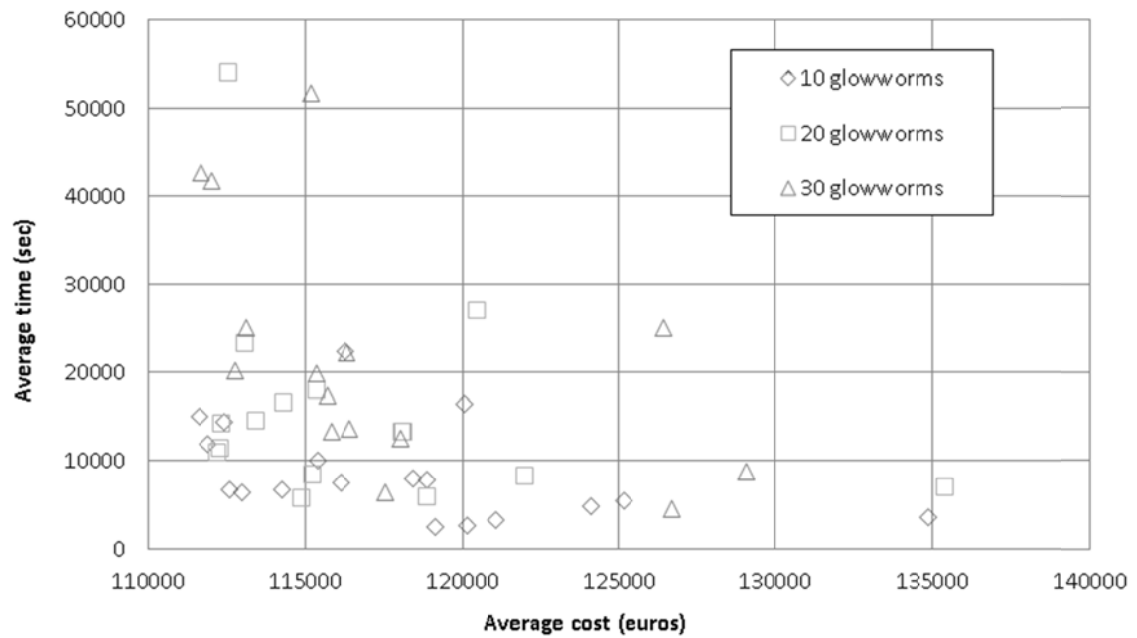**Fig. 5.** CO_2 emissions and computing time for the best solutions

Fig. 6. Cost and computing time for the best solutions
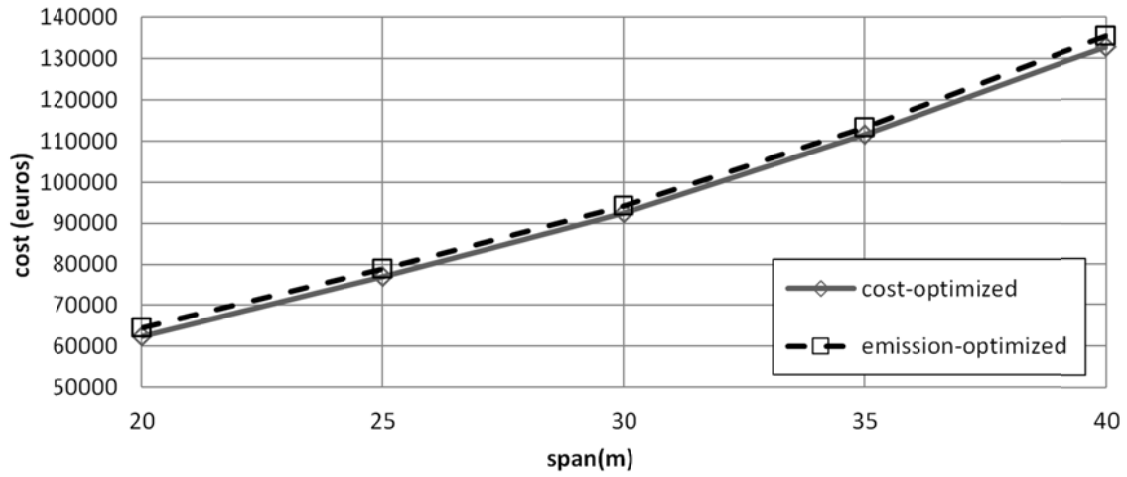
Fig. 7. Variation in the best values for minimum cost for the PC bridge studied
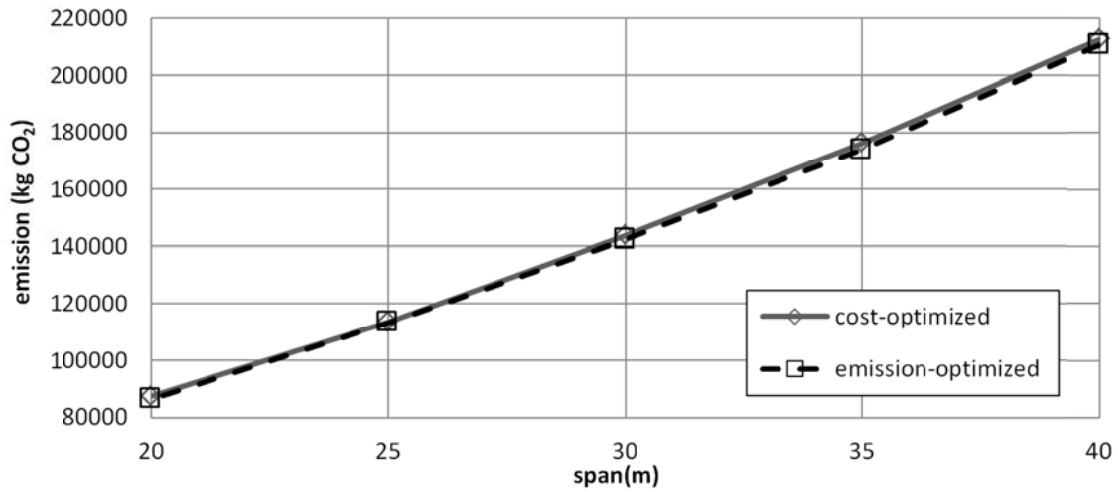
Fig. 8. Variation in the best values for the minimum CO_2 emissions for the PC bridge studied

Fig. 9. Relationship between CO_2 emissions and cost
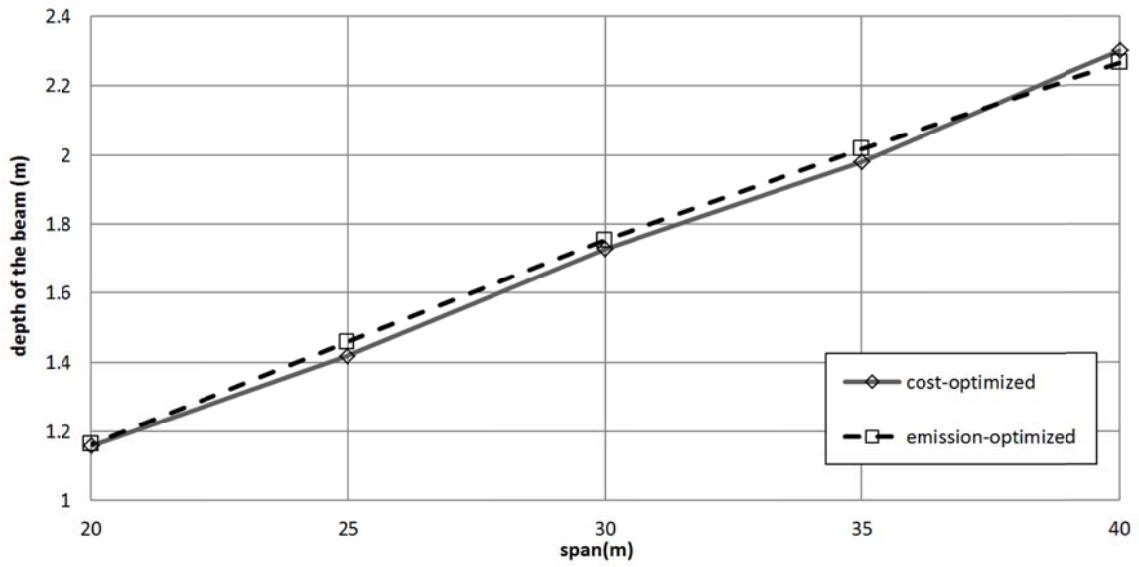
Fig. 10. Mean beam depth for different span lengths
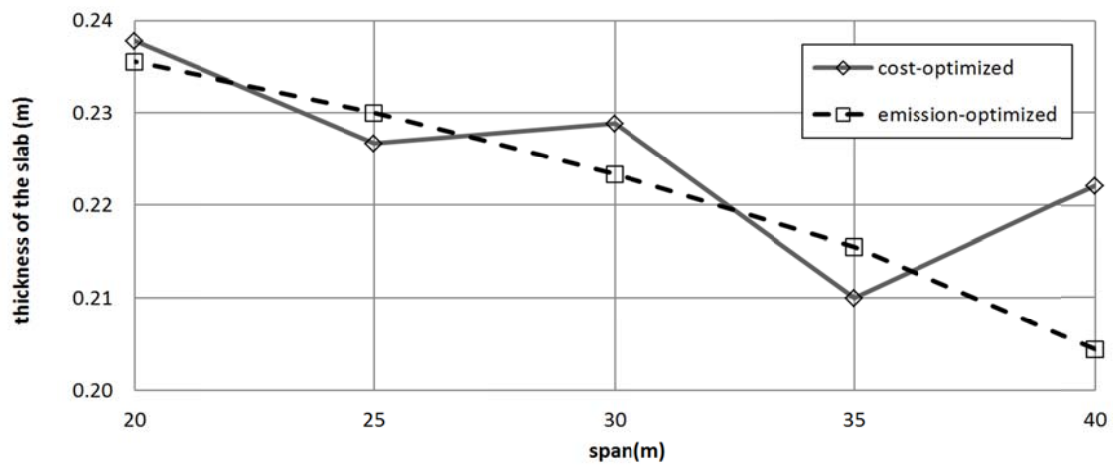
Fig. 11. Mean slab thickness for different span lengths
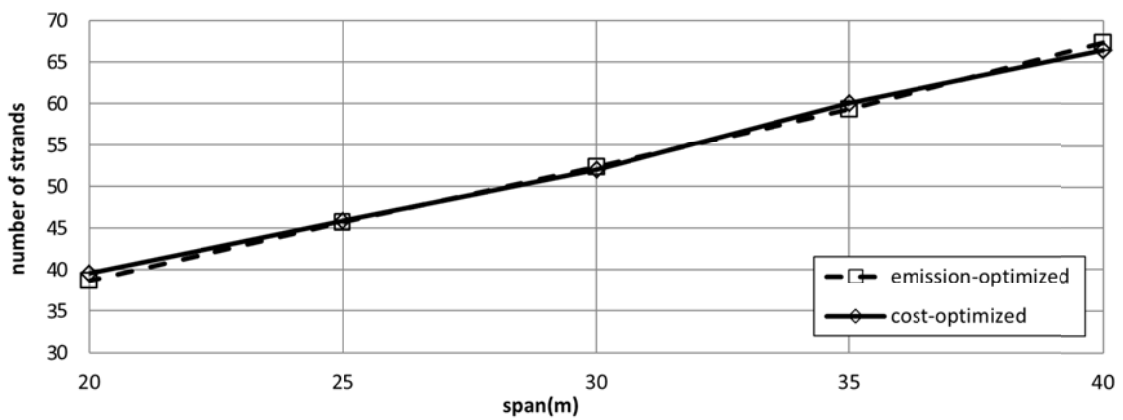
Fig. 12. Average number of strands for different span lengths
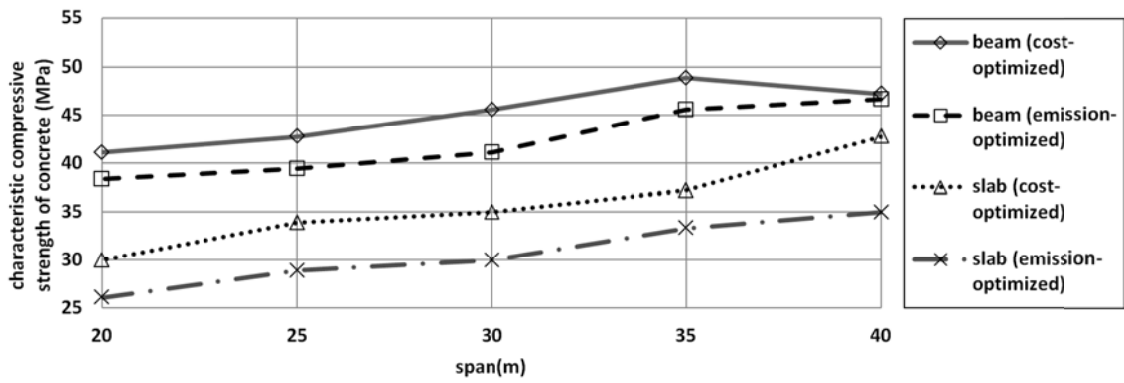
Fig. 13. Mean strength of concrete for different span lengths
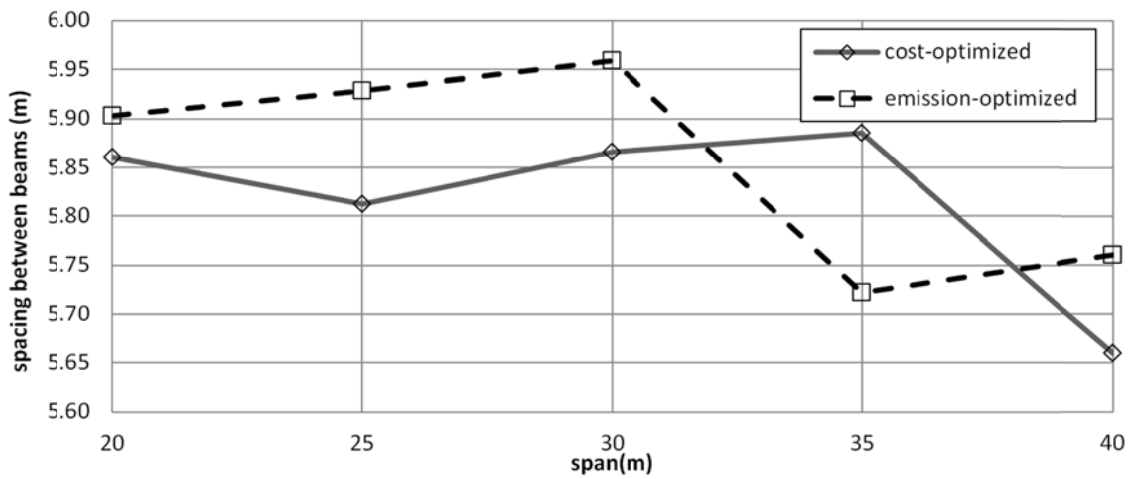
Fig. 14. Mean spacing between beams for different span lengths

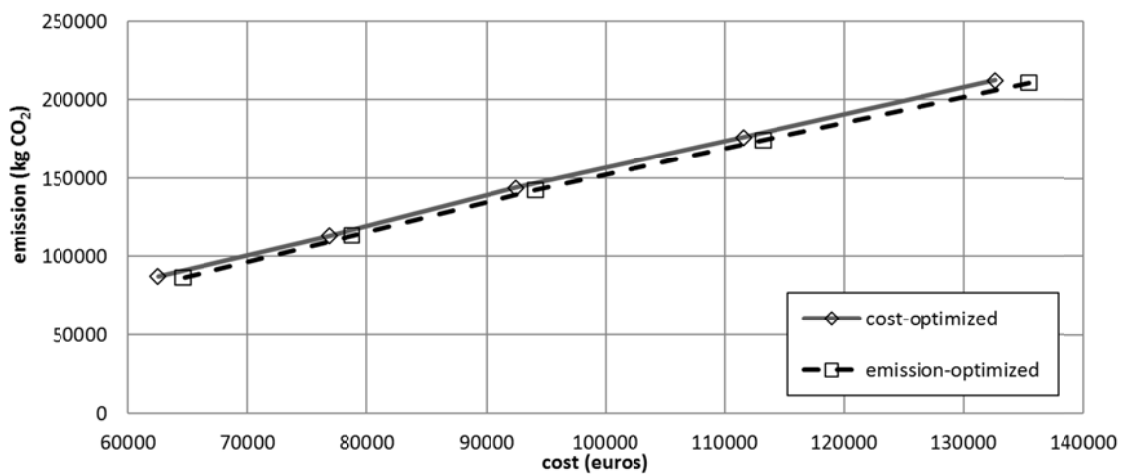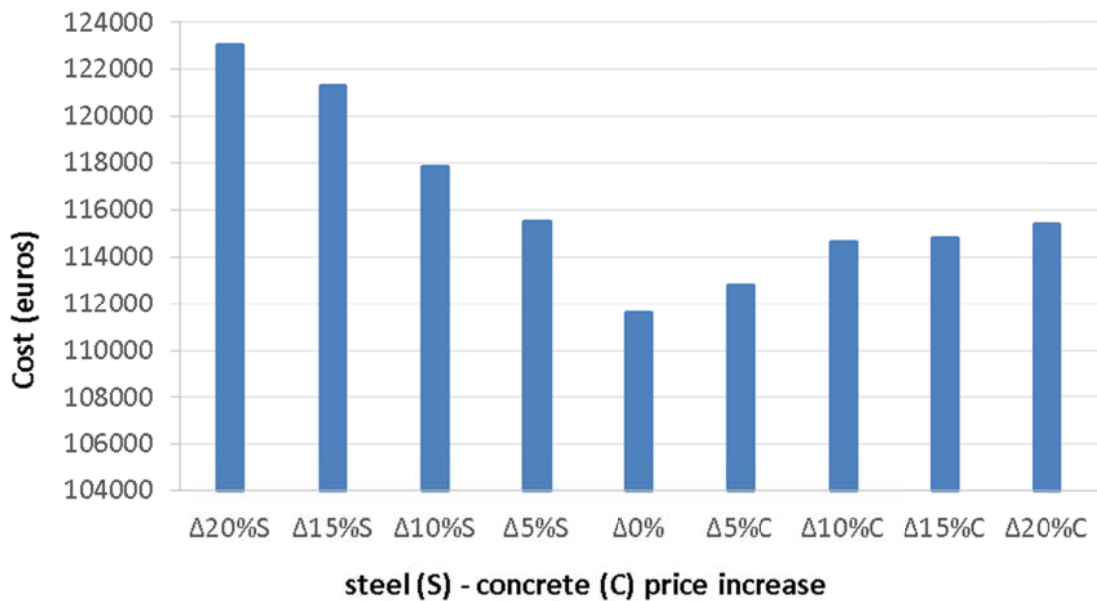**Fig. 15.** Variation in the cost for a PC precast bridge (35 m span) for increases in steel and concrete prices

Fig. 16. Variation in the steel reinforcement in relation to the surface of the slab for a PC bridge (35 m span) for increases in steel and concrete prices
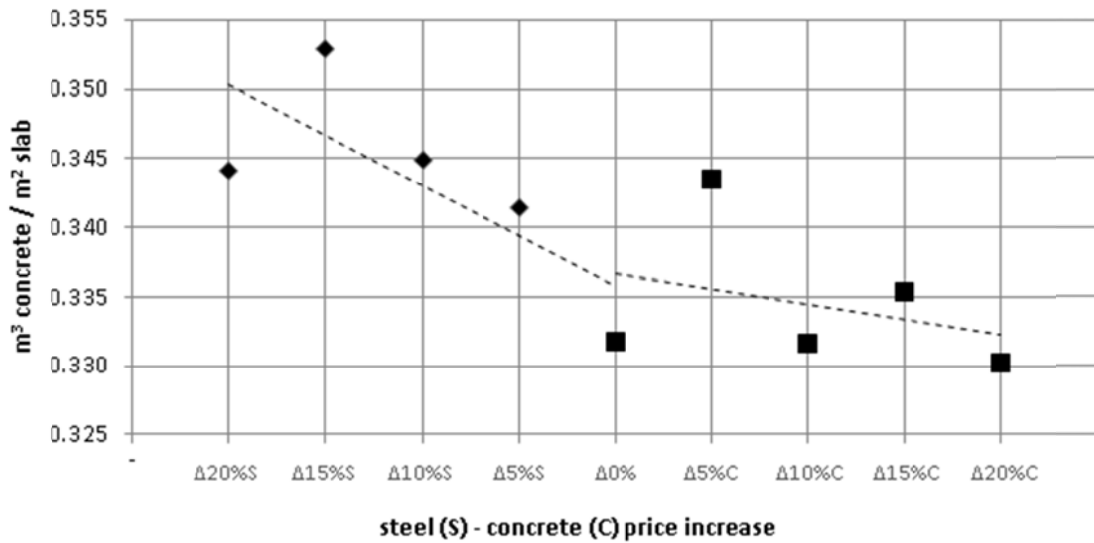
Fig. 17. Variation in the volume of concrete in relation to the surface of the slab for a PC bridge (35 m span) for increases in steel and concrete prices

Table 1. Unit prices and CO_2 emissions of the PC precast bridge

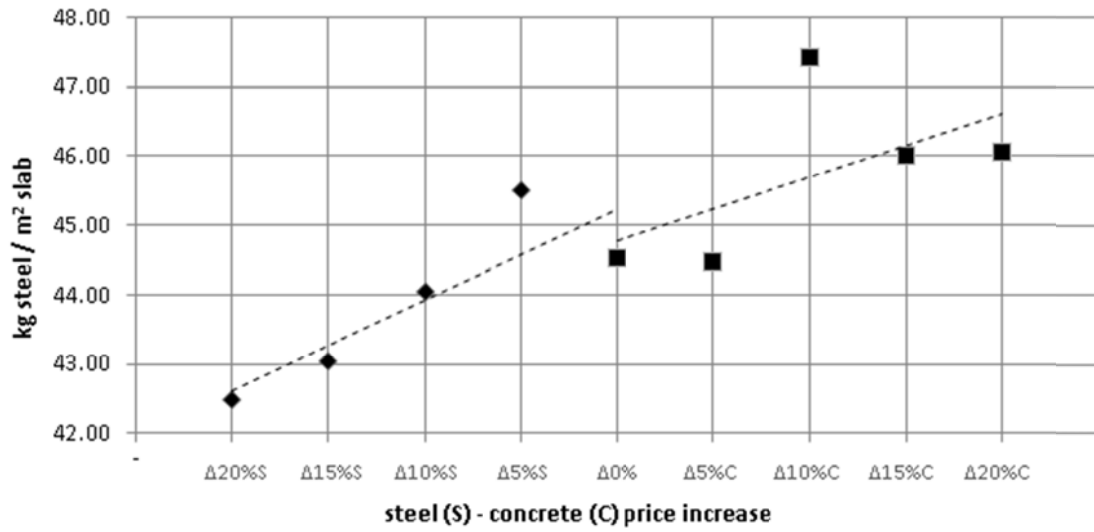| Unit	Description	Cost (€)	CO_2 emission (kg)
kg	beam steel (B-500-S)	2.88	3.03
kg	slab steel (B-500-S)	1.53	3.03
kg	active steel (Y1860-S7)	3.70	5.64
m	beam formwork	82.17	-
m^2	beam formwork	-	2.24
m^2	slab formwork	32.82	41.90
m^3	slab concrete HA-25	64.99	247.13
m^3	slab concrete HA-30	69.95	278.09
m^3	slab concrete HA-35	74.03	307.11
m^3	slab concrete HA-40	79.12	334.19
m^3	slab concrete HA-45	83.64	359.33
m^3	slab concrete HA-50	88.29	382.53
m^3	slab concrete HA-55	92.93	403.79
m^3	slab concrete HA-60	97.58	423.11
m^3	slab concrete HA-70	106.88	455.94
m^3	slab concrete HA-80	116.17	481.00
m^3	slab concrete HA-90	125.46	498.30
m^3	slab concrete HA-100	134.76	507.84
m^3	beam concrete HP-35	133.74	263.96
m^3	beam concrete HP-40	145.94	298.57
m^3	beam concrete HP-45	155.51	330.25
m^3	beam concrete HP-50	167.26	358.97
m^3	beam concrete HP-55	178.14	384.76
m^3	beam concrete HP-60	189.16	407.59
m^3	beam concrete HP-70	211.18	444.43
m^3	beam concrete HP-80	233.21	469.49
m^3	beam concrete HP-90	255.23	482.77
m^3	beam concrete HP-100	277.26	484.27

Table 2. CO_2 emissions from beam transportation and placement (distance up to 50 km, one way)

Maximum beam length (m)	Transport emissions (kg CO_2/t)	Placement emissions (kg CO_2/m)
20	76.38	39.43
25	80.12	50.24
30	98.25	61.05
35	95.38	65.18
40	93.00	69.31

Table 3. Basic prices for beam placement

Maximum beam length (m)	Placement cost (€)
20	3172.57
25	3281.97
30	5579.35
35	5688.74
40	6782.73

Table 4. Basic prices for beam transport (until 50 km)

Maximum beam weight (kN)	Transport cost (€)
550	1066.64
660	1394.84
800	1805.08
1000	1996.53
2000	3090.52
4000	4184.51

Table 5. Input parameters for the analysis

Geometric parameters	
PC precast bridge width	$W = 12.00$ m
Inclination, top flange tablet	$n_{s3} = 3$
Top flange division	$s_3 = 3$
Inclination, bottom flange tablet	$n_{i3} = 3$
Bottom flange division	$i_4 = 4$
Web inclination	80º
Minimum beam slenderness	$L/17$
Bearing center to beam face distance	0.47 m
Loading parameters	
Concrete bridge barrier width	2x0.50 m
Thickness of the wearing surface	$t_{ws} = 0.09$ m
Concrete bridge barrier loads	2x5.0 kN/m
Cost parameters	
Transport distance (one way)	$T_d = 50$ km
Active prestressing steel crops	25%
Reinforcement parameters	
Passive reinforcing steel (B-500-S)	$f_{yk} = 500$ N/mm^2
Active prestressing steel (Y1860-S7)	$f_{pk} = 1700$ N/mm^2
Strand diameter	$\Phi_s = 0.6$"
Beam surface reinforcement	$\Phi_r = 8$ mm
Strand sheaths	Levels 2 and 3
Vertical slenderness of stirrups	200 (length/diameter)
Legislative parameters	
Code regulation	EHE/IAP-98
Exposure parameters	
External ambient conditions	IIb (EHE)

Table 6. Results for the parameters calibration using CO_2 emissions as objective function

	S1	S2	S3	S4	S5	S6
Standard deviation (kg CO_2)	2734.79	4272.47	1096.96	1885.74	2315.93	1607.82
Minimum emission (kg CO_2)	170002.39	170903.20	171164.25	171736.11	172432.22	173214.53
Average emission (kg CO_2)	173525.88	176247.39	172431.52	173679.07	174076.10	174664.75
Coefficient of variation (%)	1.58%	2.42%	0.64%	1.09%	1.33%	0.92%
Average time (sec)	29323.88	7431.85	48857.71	15379.80	14710.80	10959.61
Number of iterations, t_{max}	15	15	15	5	10	5
Number of glowworms, n	10	10	30	20	10	10
Number of neighbors, n_t	10	10	10	15	10	5
Initial luciferin value, l_0	70000	50000	70000	70000	70000	70000
Radial sensor range, r_s	70	70	50	50	30	50
Luciferin value decay constant, ρ	0.50	0.70	0.70	0.70	0.50	0.50
Luciferin enhancement constant, γ	0.50	0.50	0.50	0.30	0.70	0.30
Constant parameter, β	0.05	0.05	0.08	0.05	0.08	0.08
Step size, s	60	50	70	60	50	70
Number of Markov chains, n_M	3	1	2	2	3	3
Coefficient of cooling, k	0.85	0.90	0.95	0.80	0.95	0.85
Markov chains, M_c	1500	1000	1000	1500	1000	1500
Percentage of the variables, n_p	10	10	10	10	10	10

Table 7. Results for the parameters calibration using cost as objective function

	S7	S8	S9	S10	S11
Standard deviation (euros)	2087.68	2287.53	1494.84	2419.80	1946.48
Minimum cost (euros)	109069.34	109341.96	111135.59	110247.95	111229.98
Average cost (euros)	111611.23	111871.68	112192.61	112594.42	112969.97
Coefficient of variation (%)	1.87%	2.04%	1.33%	2.15%	1.72%
Average time (sec)	15049.84	11996.38	11036.38	6732.5	6446.75
Number of iterations, t_{max}	15	10	15	15	5
Number of glowworms, n	20	10	20	10	10
Number of neighbors, n_t	15	10	5	5	5
Initial luciferin value, l_0	50000	50000	50000	70000	50000
Radial sensor range, r_s	70	50	70	50	50
Luciferin value decay constant, ρ	0.50	0.5	0.3	0.7	0.7
Luciferin enhancement constant, γ	0.3	0.3	0.7	0.3	0.3
Constant parameter, β	0.05	0.08	0.08	0.05	0.08
Step size, s	40	40	40	60	50
Number of Markov chains, n_M	2	3	1	2	2
Coefficient of cooling, k	0.85	0.80	0.8	0.9	0.8
Markov chains, M_c	1500	1500	1000	500	1500
Percentage of the variables, n_p	10	10	10	10	10

Table 8. Basic measurements of best emission (a) and best cost (b) optimized solutions for 20-25-30-35-40 m spans

Span (m)		Beam reinforcement (kg)	Slab reinforcement (kg)	Total reinforcement (kg/m^2)	Beam concrete (m^3/m^2)	Slab concrete (m^3/m^2)
20	(a)	2943	5731	34.420	0.103	0.309
	(b)	2403	8317	42.541	0.096	0.229
25	(a)	3928	6886	34.661	0.110	0.269
	(b)	3189	9959	42.143	0.108	0.200
30	(a)	4908	7536	33.452	0.119	0.280
	(b)	4640	11205	42.594	0.113	0.220
35	(a)	6892	10077	39.280	0.132	0.210
	(b)	5743	13045	43.490	0.120	0.190
40	(a)	7353	13999	43.398	0.142	0.180
	(b)	8189	11963	40.959	0.135	0.230